Chapter 3

Application of PANN

3.1 Proton-Proton Scattering at $T_L = 25 - 500$ MeV

Abstract. Modified phase-shift analyses of *p-p* scattering in the laboratory energy range from 25 to 500 MeV were carried out with the latest experimental database. The one-pion exchange amplitude, which was used for evaluation of the peripheral part of *p-p* scattering amplitude, was left unfixed, along with the phase shifts of low partial waves in the χ^2-minimizing fit to the data. The value determined for the pion-proton coupling constant is $g^2_{\pi^0 pp}/4\pi = 13.52 \pm 0.23$.
(Prog. Theor. Phys. **105** (2001), 233.)

3.1.1 Introduction

In the usual phase-shift analysis of nucleon-nucleon (N-N) scattering, which is called the modified phase-shift analysis (PSA), the peripheral part of the scattering amplitude in the outer region of the nuclear distance $r \geq 2.5$ fm is provided by the one-pion-exchange (OPE) contribution[5]. In our previous modified phase-shift analyses of $N-N$ scattering in the laboratory incident-energy region $T_L = 500 \sim 1090$ MeV[13, 42, 39], the pion-proton (πpp) coupling constants were taken as $g^2/4\pi = (2M/m)^2 f^2 = 14.4$, where $g^2/4\pi$ and f^2 are the non-derivative and derivative coupling constants, respectively, and M and m are the nucleon and the pion masses, respectively.

Even now, the method of evaluation of $g^2/4\pi$ differs slightly between groups[43, 44, 45]. Determinations of the πpp coupling constants have been carried out by Chew[46], Sawada et al.[6, 47], Ino et al.[48], Bugg[49], Grein et al.[50], Nijmegen group[43, 51], Hoshizaki et al.[44], Arndt at al.[45, 52], and Wissink[53]. The exact determination of $g^2/4\pi$ is important not only in nuclear physics but also in the hadron physics.

In 1998, the *p-p* analyzing power and spin correlation data between 200 and 450 MeV were measured by the IUCF group[54]. At $T_L = 25.68$ MeV, we have the extremely precise data of spin-correlation obtained by the PSI group in 1994. The accumulation of *p-p* scattering data at $T_L = 25 \sim 500$ MeV is very excellent.

Here we carry out the energy-independent PSA of *p-p* scattering in the region of $T_L = 25 \sim$

500 MeV using our proposed χ^2-mapping method in order to find both best fit solutions of the phase shifts and the peripheral amplitude with unfixed $g^2_{\pi^0 pp}/4\pi$ value, simultaneously. In subsection 3.1.2, we report the experimental data used in the present analysis. In subsection 3.1.3, we give the solutions of the phase shifts and the $g^2_{\pi^0 pp}/4\pi$ value. Subsection 3.1.4 is devoted to concluding remarks.

3.1.2 Experimental data used in analyses

The experimental data for p-p scattering below the laboratory energy $T_L = 510$ MeV were collected from papers published between 1950 and 1998. This database consists of 1,477 $d\sigma/d\Omega$ data points, 1,326 $P(\theta)$ data points and 2,463 spin-correlation data points, which is a total of 5,266 data points. In Fig. 3.1, we give the distribution maps of the experimental data for $d\sigma/d\Omega$, $P(\theta)$ and spin-correlations, respectively, with the horizontal axis corresponding to the laboratory kinetic energy T_L $(0-510$ MeV) and the vertical axis corresponding to the scattering angle in the center-of-mass system θ_{hboxcm} $(0-150$ degree).

In order to perform the single-energy PSA, we need a database that is close to "complete" at each energy. From the distribution maps, we find sufficient data at T_L=25, 50, 140, 210, 310, 400, 445 and 500 MeV, which are selected as the energy points for our PSAs. The observables and the corresponding number of experimental data used in the present analysis at each energy are listed in Table 3.1. Here, the expressions of observables by the spin directions (beam, target; scattered, recoil) in the laboratory system are $P = (N,0;0,0) = (0,N;0,0) = (0,0;N,0) = (0,0;0,N)$, $D = (N,0;N,0)$, $A = (L,0;S,0)$, $A' = (L,0;L,0)$, $R = (S,0;S,0)$, $R' = (S,0;L,0)$, $A_{ij} = (i,j;0,0)$, $D_{ij} = (0,0;i,j)$, $K_{ij} = (i,0;0,j)$ and $M_{ijk} = (i,j;k,0)$, where i, j and k denote the three directions of measured spin (N, L or S). Here L denotes the longitudinal direction of the beam. N denotes the normal to the scattering plane, and S denotes the $N \times L$ directions. The following criteria were adopted for the selection of database at each energy. We take the energy bins $\Delta T_L = \pm 10$ MeV for the $d\sigma/d\Omega$ data selection and $\Delta T_L = \pm 5$ MeV for other spin-correlation data selections.

The forward observables are the total cross section σ_t, the reaction cross-section σ_r, the cross section difference in the longitudinal spin states $\Delta\sigma_L$ and the cross section difference in the transverse spin states $\Delta\sigma_T$. All of them were measured at $T_L = 25, 50, 400, 445$ and 500 MeV. At 210 and 310 MeV, $\Delta\sigma_L$ and $\Delta\sigma_T$ were not measured. The number of the data points used in a single energy PSA at each energy is given in Table 3.1.

3.1.3 Solution of phase shifts and $g^2_{\pi^0 pp}/4\pi$ coupling constant

The modified phase-shift analysis of N-N scattering, in which the peripheral part of the amplitudes is evaluated using the one-pion exchange contribution, was proposed by Moravscik[4, 55] and generalized to the inelastic region by Hoshizaki[7]. The scattering amplitude is represented by the partial wave amplitudes as follows:

$$M = \sum_{\ell \le \ell < \ell_0)} f_\ell(\delta_\ell, \eta_\ell) + \sum_{\ell_0 < \ell < \ell_1} f_\ell(\delta_\ell{}^{OPE}, \eta_\ell) + M^{OPE}(\ell \ge \ell_1). \tag{3.1}$$

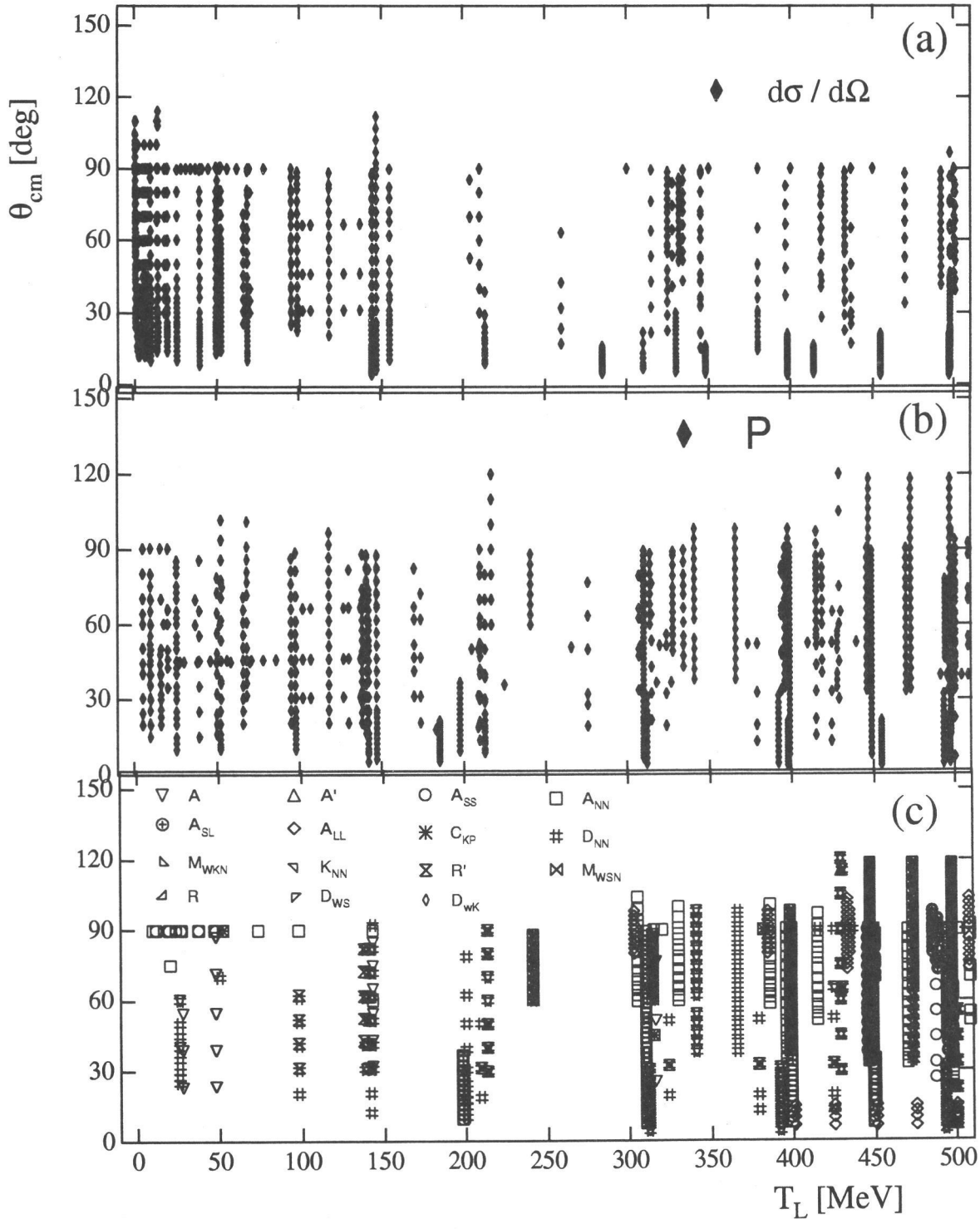

Figure 3.1: The distributions of the experimental data of p-p scattering in the T_L - θ_{cm} plane below 510 MeV. The graphs (a), (b) and (c) describe $d\sigma/d\Omega$, $P(\theta)$ and the spin-correlation parameters.

Table 3.1: The observables and the corresponding number of experimental data points used in the single-energy phase-shift analysis at each energy.

T_L (MeV)	25	50	140	210	310	400	445	500
Forward Obs.	4	4		2	2	4	3	3
$d\sigma/d\Omega$	23	72	47	7	14	39	43	97
P	24	39	105	58	82	118	103	189
R	8	5	14	15	27	29	22	43
A	5	10	12	14	24	29	19	48
R'			11	11				12
A'				5			2	16
D_{NN}	8	1	19	20	19	13	17	43
A_{NN}	1	3	2		57	58	59	34
A_{LL}					10	4	17	40
A_{SL}		1			40	40	54	23
A_{SS}	3	2			40	40	63	22
K_{NN}					8	16	28	24
M_{WSN}					8	16	24	24
M_{WKN}					8	16	21	21
D_{WS}							22	24
D_{WK}							24	24
Total	76	137	210	132	339	422	521	687

Forward Observables : σ_t, σ_r, $\Delta\sigma_T$, $\Delta\sigma_L$.

Here, ℓ is an orbital angular momentum, δ_ℓ a phase shift, and η_ℓ a reflection parameter. The boundary angular momentum ℓ_0 corresponds to the impact parameter equal to 2.5 fm, which is the effective range of the one-pion-exchange potential. ℓ_1 is appropriately determined in the process of performing the PSA.

We carried out the PSA by using the representation of the S matrices proposed by Matsuda and Watari[29] as follows. In the case $\ell = J$,

$$S_J = \eta_{\ell,J} \exp(2i\delta_{\ell,J}), \tag{3.2}$$

where $\delta_{\ell,J}$ is the nuclear-bar phase shift and $\eta_{\ell,J}$ the reflection parameter. In the case $\ell = J \pm 1$,

$$S_J = \begin{bmatrix} \sqrt{1 - |\rho_J|^2}\eta_- \exp(2i\delta_-) & i\rho_J\sqrt{\eta_-\eta_+}\exp[i(\delta_- + \delta_+)] \\ i\rho_J\sqrt{\eta_-\eta_+}\exp[i(\delta_- + \delta_+)] & \sqrt{1 - |\rho_J|^2}\eta_+ \exp(2i\delta_+) \end{bmatrix}, \tag{3.3}$$

where $\delta_\pm \equiv \delta_{J\pm1,J}$ and $\eta_\pm = \eta_{J\pm1,J}$ are the phase shifts and reflection parameters, and ρ_J is the parameter of the wave mixing. $\eta_{\ell,J} = 1.0$ in the energy region, where no inelastic channels are opened. The software developed for this PSA was published by Matsuda et al.[57].

The partial wave amplitudes with $\ell > \ell_0$ in Eq. (3.1) were calculated using the OPE amplitude. The S matrices are related to the amplitudes $\alpha_{\ell,J}[f_\ell(\delta_\ell, \eta_\ell)]$ by

$$\alpha_{\ell,J} = \frac{1}{2ik}(S_{\ell,J} - 1). \tag{3.4}$$

The partial wave amplitudes $\alpha_{\ell,J}$ of OPE contribution are given by

$$\alpha_\ell = i\frac{kg^2_{\pi^0 pp}}{2E}[(x_0-1)Q_\ell(x_0) - \delta_{\ell 0}], \tag{3.5}$$

$$\alpha_{J-1,J} = -i\frac{kg^2_{\pi^0 pp}}{2E(2\ell+3)}[Q_{\ell+1}(x_0) - Q_\ell(x_0)], \tag{3.6}$$

$$\alpha_{J+1,J} = -i\frac{kg^2_{\pi^0 pp}}{2E(2\ell-1)}[Q_\ell(x_0) - Q_{\ell-1}(x_0)], \tag{3.7}$$

$$\alpha_{J,J} = -i\frac{kg^2_{\pi^0 pp}}{2E(2\ell+1)}[\ell Q_{\ell+1}(x_0) + (\ell+1)Q_{\ell-1}(x_0) - (2\ell+1)Q_\ell(x_0)], \tag{3.8}$$

$$\alpha^J = -i\frac{kg^2_{\pi^0 pp}}{2E(2\ell+1)}\sqrt{J(J+1)}[Q_{J+1}(x_0) + Q_{J-1}(x_0) - 2Q_J(x_0)], \tag{3.9}$$

$$x_0 = 1 + \frac{m^2_{\pi^0}}{2k^2}. \tag{3.10}$$

Here, k is the proton momentum in the center-of-mass system, Q_J is the associated Legendre function, and m_{π^0} is the neutral-pion mass.

A best fit solution of partial wave amplitudes is obtained by varying the free parameters so as to minimize the χ^2-value:

$$\chi^2 = \sum_{i,j}\left[\frac{\theta^{th}_{i,j} - n_j\theta^{ex}_{i,j}}{\Delta\theta^{ex}_{i,j}}\right]^2 + \sum_j\left[\frac{1-n_j}{\Delta n_j}\right]^2, \tag{3.11}$$

where $\theta^{ex}_{i,j}$ is the experimental datum for observable i from the jth experiment, with experimental error $\Delta\theta^{ex}_{i,j}$, and $\theta^{th}_{i,j}$ is its theoretical value. Here n_j and Δn_j are the experimental renormalization parameter and the statistical error assigned to the experimental data of the jth group. n_j is used as a free parameter only for some data regarding the differential cross section, for which extreme differences among the data sets exist.

We carried out the PSA by taking the $\delta_{\ell,J}$ values obtained from SAID[58] as the initial values. In the χ^2-minimizing search, we determined reasonable values of the boundary angular momentum ℓ_0 and the coupling constant $g^2_{\pi^0 pp}/4\pi$ (abbreviated as g^2) by the following χ^2-mapping method:

(1) The approximate value of ℓ_0 is evaluated by the equation $b = \sqrt{\ell_0(\ell_0+1)}/p$, where the impact parameter b is equal to 2.5 fm. This value is called $\ell_0^{(1)}$.

(2) By taking $\ell_0 = \ell_0^{(1)}$, we carry out the PSA at 10 or 11 values of g^2 from 11.5 to 16.0, and plot the χ^2-values for the solutions obtained in the $\chi^2 - g^2$ plane, as is seen in Fig. 3.2.

(3) By taking ℓ_0 as a value close to $\ell_0^{(1)}$, we once again perform step (2). In this case the ℓ_0 value is called as $\ell_0^{(2)}$. We repeat this several times using different values of $\ell_0, \ell_0^{(n)} (n = 1, 2, 3, \cdots)$.

(4) When we use some $\ell_0^{(n)}$ larger than the proper value ℓ_0, we obtain a flat χ^2 valley. On the other hand, using the $\ell_0^{(n)} \leq \ell_0$, we get some depressed χ^2 valleys. Here the

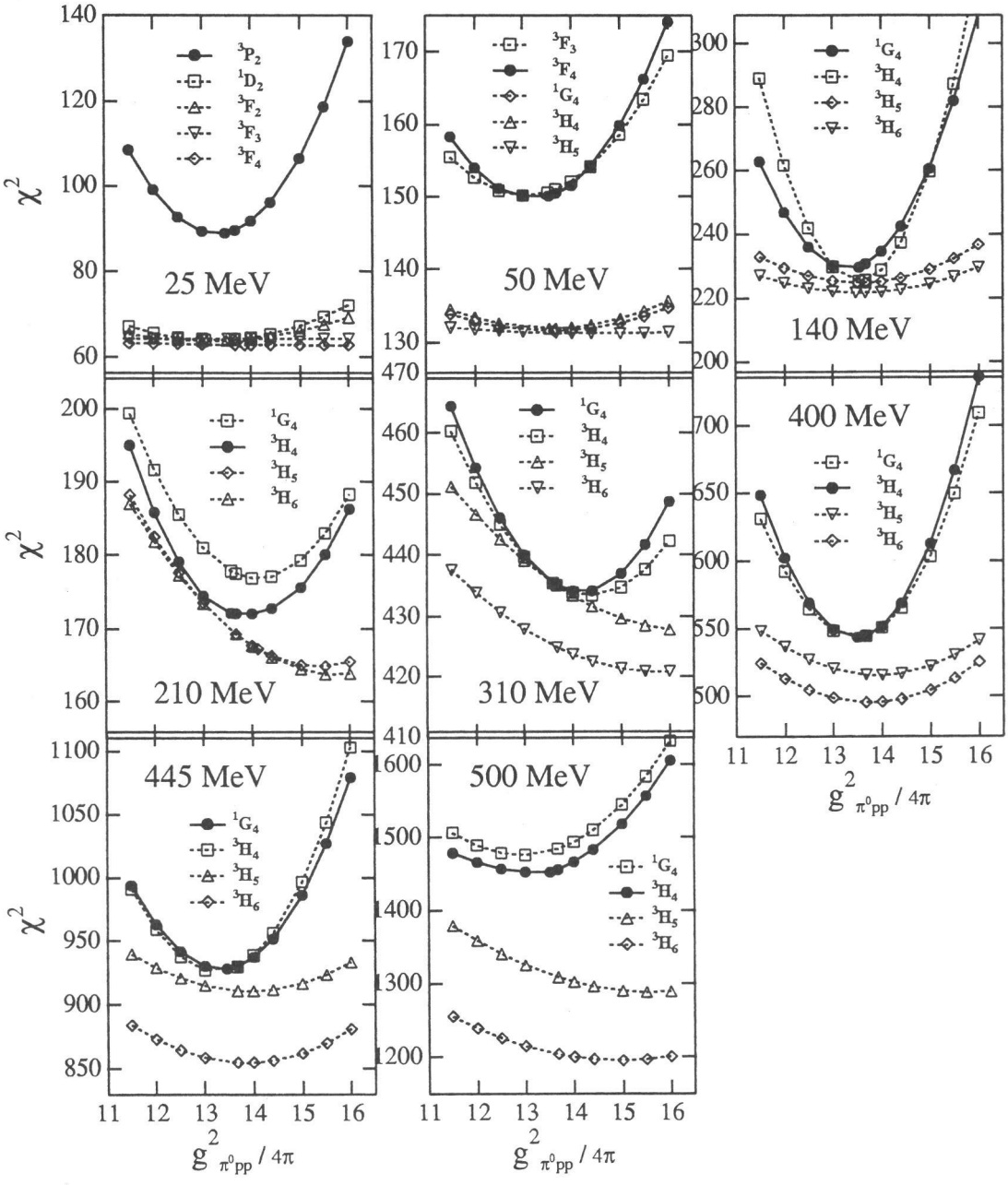

Figure 3.2: The $\chi^2 - g^2$ maps in the χ^2 minimization for each value of the boundary angular momentun ℓ_0. From the maps, the best values of ℓ_0 are found to be $^3P_2$ at 25 MeV, $^3F_4$ at 50 MeV, $^1G_4$ at 140 MeV, $^3H_4$ at 210 MeV, $^1G_4$ at 310 MeV, $^3H_4$ at 400 MeV, $^1G_4$ at 445 MeV and $^3H_4$ at 500 MeV.

deepest χ^2 valley corresponds to the proper value of ℓ_0, the minimum value of which corresponds to the most reasonable value of g^2 with the present experimental database.

(5) We obtain the final solution for $\delta_{\ell,J}(\ell \leq \ell_0)$ and g^2 by carrying out the PSA where the values of $\delta_{\ell,J}$ and g^2 obtained in step (4) are taken for the starting values of the free parameters.

The obtained $\chi^2 - g^2$ maps are shown in Fig. 3.2. At $T_L = 140$ MeV, for example, all of the χ^2 valleys with $\ell_0 = {}^3H_5$ and ${}^3H_6$ are flat, and those with $\ell_0 = {}^1G_4$ and ${}^3H_4$ have the depressed shapes. We thus obtain the solution of $\delta_{\ell,J}$ about $(\ell, J) \leq^1 G_4$ with $g^2_{\pi^0 pp}/4\pi = 13.54 \pm 0.22$. The obtained solutions for phase shifts at $T_L = 25$, 50, 140, 210, 310, 400, 445 and 500 MeV are given in Table 3.2. The value determined for $g^2_{\pi^0 pp}/4\pi$ at each energy is given in Table 3.3. In this table, the final values of g^2 almost coincide with the g^2 values corresponding to the minima of χ^2 in Fig. 3.2, except for those at 310 and 500 MeV.

Our present solutions for the phase shifts and mixing parameters are shown in Fig. 3.3, together with the results of the phase-shift analysis of Bergervoet et al.[43], Arndt et al.[59], Dubois et al.[60], Bugg et al.[61] and the energy-dependent solutions of the Nijmegen[43] and VPI[45] groups. Our mixing-parameter ρ_J is related to that of Stapp[37], ε_J, according to $\varepsilon_J = \frac{1}{2}\sin^{-1}\rho_J$. The parametrization of Arndt et al.[30] is based on the K-matrix. The equation $S = (1 + iK)/(1 - iK)$ relates our amplitudes to those given by Arndt et al.[30].

3.1.4 Concluding remarks

We have carried out single energy PSA for p-p scattering using the most recent database at 8 points of the incident energy below 500 MeV and have precisely determined the $\pi^0 pp$ coupling constant with the χ^2 mapping method. The experimental database we used consists of 22 forward-observable data, 342 for $d\sigma/d\Omega$, 718 for $P(\theta)$ and 1,442 for the spin-correlation parameters (total 2,524). We obtained almost unique solutions for the phase shifts at each energy below 310 MeV. At 100 MeV, we have plentiful data on the spin-correlation coefficients, but we do not have data on $d\sigma/d\Omega$ at small angles. For this reason, we excluded the solution at this energy from the present result. Above 400 MeV, the reflection parameters $\eta_{\ell,J}$ for low partial waves must be searched with the phase shifts, owing to opening of inelastic channels. We need more data on many kinds of spin-correlation observables in this energy region in order to remove the ambiguities found in the solutions for $\delta({}^3H_4)$ and ρ_4. The average value of $g^2_{\pi^0 pp}/4\pi$ obtained in the present analysis is 13.52 ± 0.23. This is compared with the values obtained by other groups in Table 3.4. The value obtained by the Nijmegen groups[43] is most consistent with our value.

In the future, we will carry out PSA for p-p scattering by using the χ^2 - mapping method in the energy region $T_L = 500 - 1,000$ MeV.

Table 3.2: The phase-shifts obtained by the present single-energy PSA at T_L = 25, 50, 140, 210, 310, 400, 445 and 500 MeV. The phase-shift values in the parentheses are those calculated by the one-pion exchange amplitude.

Waves	T_L = 25 (MeV) χ^2/N_t = 89/76	T_L = 50 (MeV) χ^2/N_t = 150/137	T_L = 140 (MeV) χ^2/N_t = 229/210
	δ	δ	δ
$^1S_0$	48.52± 0.26	39.22 ± 0.13	17.31 ± 0.18
$^3P_0$	9.45± 0.20	12.58 ± 0.13	7.22 ± 0.08
$^3P_1$	−4.70± 0.18	−7.16 ± 0.12	−16.84 ± 0.20
$^3P_2$	2.36 ± 0.12	5.66 ± 0.08	13.61 ± 0.17
ε_2	(−0.014)	−0.058 ± 0.10	−0.010 ± 0.13
$^1D_2$	(0.56)	1.58 ± 0.03	5.12 ± 0.06
$^3F_2$	(0.11)	0.12 ± 0.07	1.21 ± 0.09
$^3F_3$	(−0.24)	−0.92 ± 0.06	−1.95 ± 0.08
$^3F_4$	(0.02)	0.04 ± 0.04	0.97 ± 0.06
ε_4	(−0.001)	(−0.003)	−0.021 ± 0.10
$^1G_4$	(0.04)	(0.15)	0.49 ± 0.05
$^3H_4$	(0.01)	(0.03)	(0.19)

Waves	T_L = 210 (MeV) χ^2/N_t = 173/132	T_L = 310 (MeV) χ^2/N_t = 435/339
	δ	δ
$^1S_0$	4.68 ± 0.52	−7.16 ± 0.46
$^3P_0$	−2.85 ± 0.47	−10.38 ± 0.46
$^3P_1$	−22.73± 0.31	−28.93 ± 0.29
$^3P_2$	16.50± 0.25	17.11 ± 0.29
ε_2	−0.088 ± 0.28	−0.079 ± 0.31
$^1D_2$	7.73 ± 0.24	9.68 ± 0.23
$^3F_2$	1.27 ± 0.26	0.84 ± 0.23
$^3F_3$	−2.60 ± 0.29	−2.99 ± 0.29
$^3F_4$	1.58 ± 0.20	2.67 ± 0.20
ε_4	−0.048 ± 0.25	−0.046 ± 0.28
$^1G_4$	0.89 ± 0.13	1.55 ± 0.21
$^3H_4$	0.26 ± 0.12	(0.55)

Waves	T_L = 400 (MeV) χ^2/N_t = 543/422		T_L = 445 (MeV) χ^2/N_t = 910/517	
	δ	η	δ	η
$^1S_0$	−13.34 ± 0.41	1.0	−20.23 ± 0.38	1.0
$^3P_0$	−18.05 ± 0.29	1.0	−22.11 ± 0.32	0.949 ±0.007
$^3P_1$	−33.89 ± 0.32	1.0	−36.69 ± 0.33	0.958 ±0.005
$^3P_2$	17.40 ± 0.23	1.0	18.04 ± 0.27	1.0
ε_2	−0.033 ± 0.31	0.0	−0.023 ± 0.31	0.0
$^1D_2$	11.34 ± 0.18	0.953±0.003	12.15 ± 0.26	0.935 ±0.003
$^3F_2$	−0.22 ± 0.23	1.0	−0.33 ± 0.28	1.0
$^3F_3$	−2.59 ± 0.23	0.995±0.001	−2.84 ± 0.25	0.974 ±0.002
$^3F_4$	3.81 ± 0.17	1.0	4.11 ± 0.20	1.0
ε_4	−0.057 ± 0.23	0.0	−0.053 ± 0.23	0.0
$^1G_4$	2.13 ± 0.12	1.0	2.89 ± 0.13	1.0
$^3H_4$	0.70 ± 0.19	1.0	(0.79)	1.0

Waves	T_L = 500 (MeV) χ^2/N_t = 1476/687	
	δ	η
$^1S_0$	−24.34 ± 0.38	1.0
$^3P_0$	−25.26 ± 0.34	0.972 ±0.007
$^3P_1$	−39.48 ± 0.30	0.961 ±0.003
$^3P_2$	18.79 ± 0.22	1.0
ε_2	−0.036 ± 0.32	0.0
$^1D_2$	13.24 ± 0.21	0.853 ±0.003
$^3F_2$	−0.63 ± 0.21	1.0
$^3F_3$	−1.69 ± 0.23	0.971 ±0.002
$^3F_4$	4.38 ± 0.16	1.0
ε_4	−0.053 ± 0.26	0.0
$^1G_4$	2.78 ± 0.15	0.999 ±0.001
$^3H_4$	0.52 ± 0.18	1.0

N_t : Total number of the data

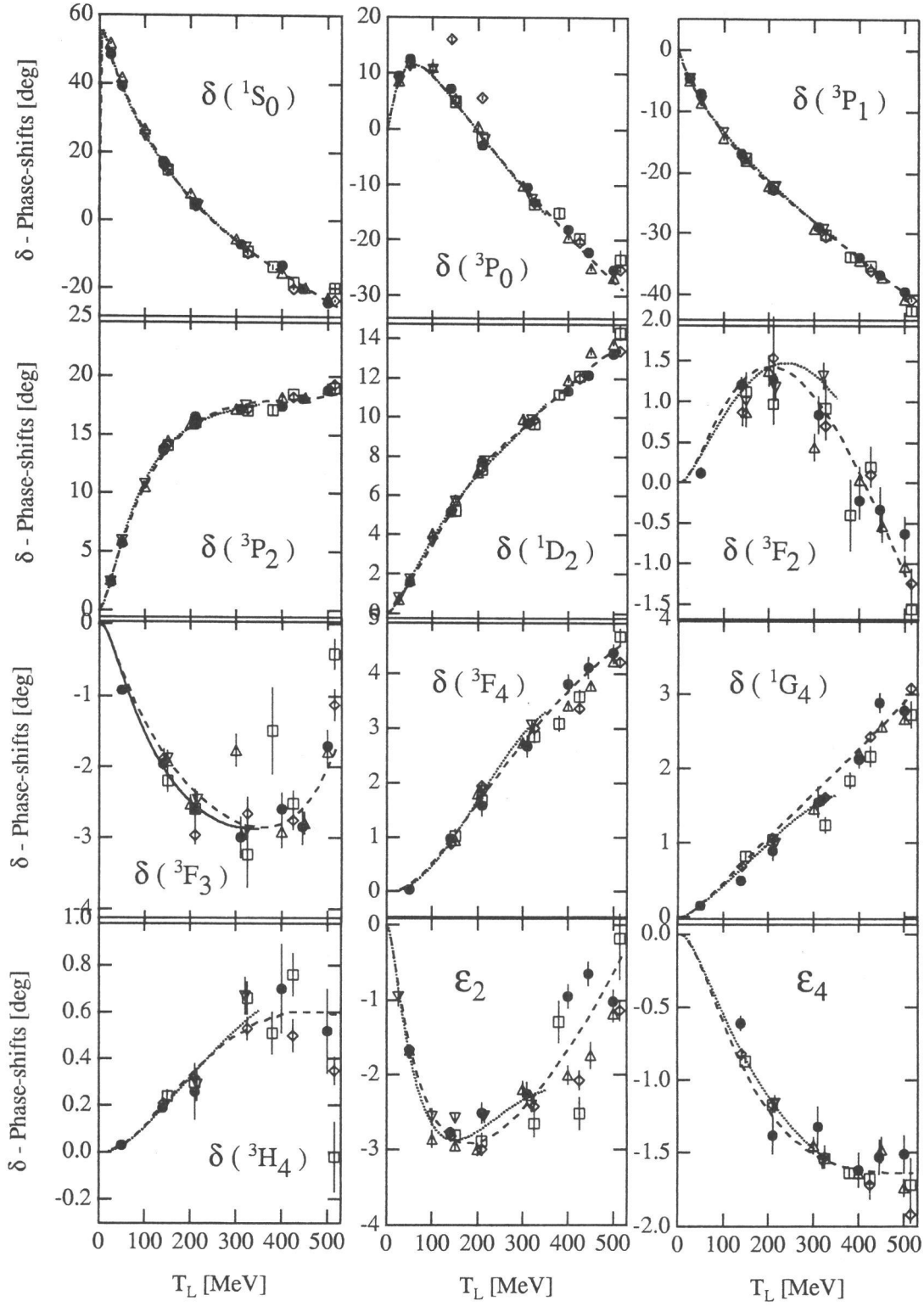

Figure 3.3: The present solutions of the phase shifts $\delta_{\ell,J}$ in degrees vs T_L in MeV and the mixing parameters ε_J, for comparison with those obtained by the other groups. Here represents • our solutions, ▽ those of Bergervoet et al.[43], △ those of Arndt et al.[59], ◇ those of Dubois et al.[60], and □ those of Bugg et al.[61]. The dotted and dashed lines are the solutions of the energy-dependent PSA by the Nijmegen[62] and VPI[63] groups, respectively.

Table 3.3: The $g^2_{\pi^0 pp}/4\pi$ values determined by the χ^2 mapping method at each energy point.

T_L (MeV)	No. of δ, η	No. of data	χ^2	$g^2_{\pi^0 pp}/4\pi$
25	4	76	89	13.47 ± 0.21
50	9	137	150	13.53 ± 0.07
140	11	210	229	13.54 ± 0.22
210	12	132	173	13.56 ± 0.36
310	11	339	434	13.58 ± 0.35
400	14	422	543	13.49 ± 0.14
445	15	521	910	13.45 ± 0.29
500	17	687	1476	13.51 ± 0.22
			(average)	13.52 ± 0.23

Table 3.4: Our value for the coupling constant ($g^2_{\pi^0 pp}/4\pi$) in comparision with the values obtained by other groups.

Groups of researcher	kind of PSA	year	$g^2_{\pi^0 pp}/4\pi$	Reference
This work	Single-energy	2000	13.52 ± 0.23	
Arndt et al.	Energy-dependent	1995	13.61 ± 0.09	[45]
Bergervoet et al.	Energy-dependent	1990	13.54 ± 0.13	[43]
Kroll et al.	(Dispersion relation)	1981	14.52 ± 0.40	[64]
Bugg et al.	Single-energy	1978	14.06 ± 0.65	[61]
Bugg et al.	(Dispersion relation)	1968	13.6 ± 0.7	[49]
MacGregor et al.	Energy-dependent	1968	14.72 ± 0.83	[56]